Volume 1 | Number 1 | Jan 2013 | Pages 1–100

Journal of
Materials Chemistry A

Materials for energy and sustainability
www.rsc.org/materialsA

Li⁺

ROYAL SOCIETY
OF CHEMISTRY

Journal of Materials Chemistry A

PAPER

Improved cycle stability and high security of Li-B alloy anode for lithium/sulfur battery

Xiaolin Zhang,[ab] Weikun Wang,[*b] Anbang Wang,[*b] Yaqin Huang,[a] Keguo Yuan,[b] Zhongbao Yu,[b] Jingyi Qiu[b] and Yusheng Yang[ab]

Lithium-sulfur (Li-S) batteries suffer from low capacity retention rate and high security risks, in large part because of the use of metal lithium as anode. Here, by employing a Li-B alloy anode, the Li-S batteries were capable of enhancing their cycle performance and security. Li-B alloy has unique structure with abundant free Li embedded in stable Li7B6 loofah sponge-like framework. The Li_7B_6 constituent functions in the following three aspects: 1) eliminates orientational crystallization of free lithium, 2) reduces effective current density and promotes the formation of SEI layers and 3) protects alloy bulk materials from deform, volume expand or collapse when cycling.

Introduction

Electrical energy storage is one of the most critical needs of 21st century society. Tremendous efforts have been devoted to developing new materials for secondary batteries, fuel cells, solar cells, and electrical double-layer capacitors [1-4]. Among these power sources, Li-ion batteries have been successfully implemented in most portable electronic devices, such as cellular phones, computers, and digital cameras, but cannot deliver the step change in energy density required in the longer term markets such as electric vehicles and electrical energy storage systems[5].

Rechargeable Li-S batteries have recently received significant attention due to their high theoretical energy density (2600 Wh/kg). In addition, sulfur is inexpensive, abundant on earth, and environmentally benign [6-7]. With these appealing features, Li-S batteries are considered to be one of the next-generation power sources in emerging advanced technologies. However, Li-S batteries have not yet been commercialized due to the following issues which need to be fully addressed before the full potential of lithium/sulfur cells can be realized: short cycle life, low charging efficiency, poor safety, and a high self-discharge rate. It seems that there is still a long way to go for the development of Li-S batteries with high specific energy, outstanding cycle stability and reliable security [8-10].

Most of the recent efforts have been focused on the sulfur-based cathode materials, such as increasing their electronical conductivity and restraining the ionic mobility of the polysulfide anions, and a series of important technological breakthroughs have been achieved [11-15]. But relatively, much fewer efforts have been made for the metal Li anode, which actually still remains a serious problem: the dendritic morphology of cycled Li resulted from uneven deposition [16-17]. On one hand, the dendrite Li will degrades the thermal stability of batteries and may lead to short circuit and even catastrophic failure; on the other hand, both fresh Li and electrolyte will be continually consumed because of the unstable solid electrolyte interface (SEI) film, and therefore decreases the cycling efficiency of the Li electrode [18]. Lee et al. [19] introduced a polymer-based protective film on the surface of metal Li by UV curing; thin lithium aluminium (Li-Al) alloy layer was formed on the Li surface to mitigate the adverse effects of polysulfide shuttle phenomenon [20], and $LiNO_3$ was used as electrolyte additive to improve the stability and uniformity of the SEI layer [21-22]. But the above approaches have not addressed the problem fundamentally.

In this work, we focused on the cycle stability and safety aspect of Li-B alloy, which could be a potential anode for rechargeable lithium batteries. Various characterizations were used to analyse the morphology and electrochemical behaviours of the Li-B alloy anode. The details of these analysis and long-term test results of LiB-S batteries were reported, while fundamental mechanisms behind the performances were analysed.

Experimental

Li-B alloy were obtained from China Energy Lithium Co. Ltd. (Tianjin, China), which had been cut into the specific size (a diameter of 14mm or a side length of 1cm).

XRD patterns of Li-B alloy (China Energy Lithium Co. Ltd.) were obtained using a Rigaku RINT2400 diffractometer with Cu Kαradiation at 40 kV and 40 mA at a step of 0.050° in the 2θ range of 10° to 90°. All the samples were sealed with Polyimide Film to avoid the exposure to outside atmosphere, hence a broad characteristic peak of Polyimide could be observed near 20°.

Three-dimensional height images of Li-B alloy samples surface were obtained in tapping mode by an AFM system (Solver P47-PRO, NT-MDT, Russia). AFM images were generated by a pixel dimension of 256×256 and a scan rate of 1Hz. Furthermore, other scanning parameters were also optimized for obtaining high-quality images. To obtain the framework image of Li_7B_6 constituent, we assembled a Li-B

alloy/Ni cell and dissolved the free Li by discharging at 0.5mA cm^{-2} for 4h. The treated alloy samples were washed with 1,2-dimethoxyethane (DME, analytically pure, water content < 3.0 × 10^{-3}%) and further dried in an argon-filled glove-box for 2 h.

The surface morphologies of electrodes were measured by scanning electron microscopy (SEM) using a HITACHI S-4700 scanning electron microscope at a working distance of 10 mm and an accelerating voltage of 20k eV. The treated samples were washed and dried as above.

The compositions of the SEI layers formed on the surfaces of Li-B alloy anodes were analysed by X-ray photoelectron spectroscopy (XPS). XPS measurements of the samples were performed with a Physical Electronics Quantera scanning X-ray microprobe with a focused monochromatic Al KαX-ray (1486.7 eV) source for excitation and a spherical section analyser. The samples were mounted onto the standard sample holder inside a nitrogen recirculated glove-box.

The electrochemical performances were evaluated using CR2025 coin-type cell. The dissolution/deposition efficiency (EFF) of Li-B alloy was tested with alloy/Ni cell. The EFF is calculated with the following equation: EFF = ($Q_{dissolution}$ / $Q_{deposition}$) × 100%, where $Q_{deposition}$ is the charge quantity of the deposited Li, $Q_{dissolution}$ is the dissolution quantity of the deposited Li.

The preparation of cathode was reported in detail elsewhere. The electrolyte was 0.6mol L^{-1} LiTFSI/DOL + DME (1:1 by volume) with 0.4mol L^{-1} LiNO$_3$ as additive. Galvanostatic charge-discharge performances were tested between 1.7 V and 2.8 V using a LAND CT2001A multi-channel battery testing system at room temperature.

The electrochemical impedance spectroscopy (EIS) were carried out with a CHI660D electrochemical analyser in the three-electrode cells, in which 1cm^2 Li-B alloy was used as working electrode, 9cm^2 lithium foil as counter electrode and lithium wire as reference electrode. The impedance spectra were recorded applying an AC voltage of 5 mV amplitude in the 0.01 Hz−100 kHz frequency range by a Solartron 1250 frequency response analyser.

Results and discussion

Figure 1a shows the XRD pattern of Li-B alloy with boron content of 30wt%. Li-B alloy is composed of two phases, rhombohedral Li$_7$B$_6$ compound (JCPDS 41-0773) and cubic lithium (JCPDS 15-0401), which is consistent with previous literature[23]. Characteristic peaks of element lithium and boron are marked beneath for comparison. To display its peculiar structure clearly, AFM images of Li-B alloy have been first observed. The pristine alloy has smooth surface with slight rolling texture (Figure 1b). After a Li dissolution step, however, some mountain-like protuberances appear (Figure 1c), indicating that after removing the free Li, Li$_7$B$_6$ constituent still remains and functions as basic framework. As discussed above, Li-B alloy has unique structure with abundant free Li embedded in stable Li$_7$B$_6$ framework.
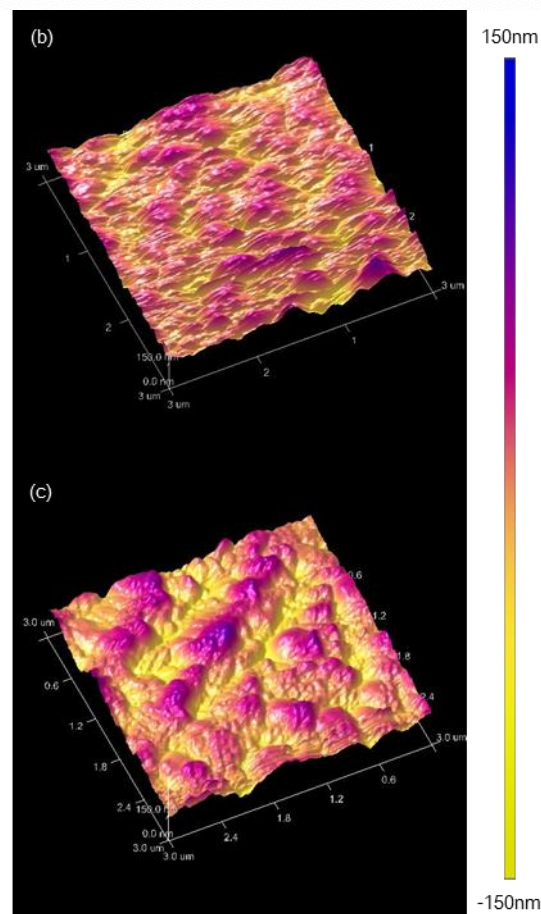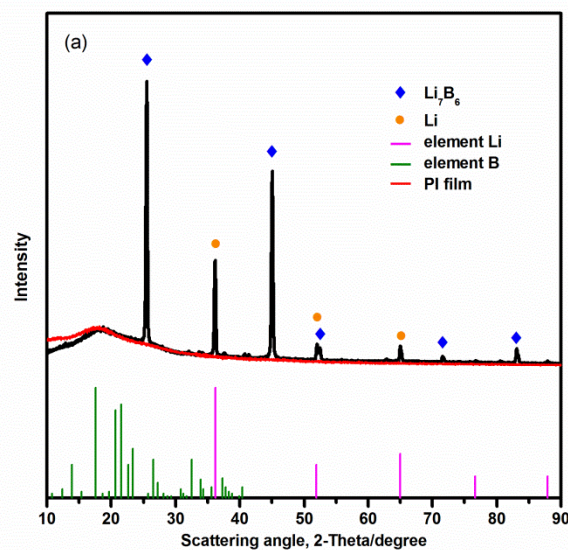
Fig.1 (a) XRD pattern of Li-B alloy with B content of 30wt%; AFM images of (b) original Li-B alloy and (c) Li-B alloy after a Li dissolution step.

Li dissolution/deposition was implemented by plating Li onto Ni foil and then deplating, employing a current of 1.0mA cm^{-2}. Shown in Figure 2 is the scatterplot of Li dissolution/deposition efficiency for 100 cycles. The experimental cell of Li-B alloy overwhelmingly

outperformed the control cell of metallic lithium. The dissolution/deposition efficiency of metallic lithium keeps steady in the first 20 cycles at ca. 90%, while it fells 7 percent precipitously at 21st cycle and begins to fluctuate slightly, reflecting a sudden change on the surface of metallic lithium. In the following 80 cycles, the serious turbulence of efficiency reach up to a rate of 30%. In contrast, the Li dissolution/deposition efficiency of Li-B alloy maintains flat during the whole long cycling over 96%.
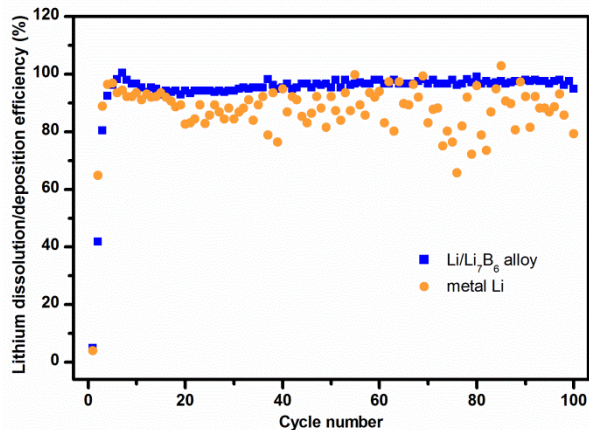
Fig.2 Cycling efficiency of lithium deposition/dissolution for Li-B alloy (30wt% B) and metal Li electrodes.

The positive effect of Li-B alloy was further verified by a comparison between LiB-S and Li-S full cells cycled at a current density of 100mA g^{-1} $_{sulfur}$. The 1st cycle charge/discharge profiles of both batteries are exhibited in Fig. 3a. It is evident from the profiles that the charge and discharge plateaus corresponded to the electrochemical reaction of LiB-S battery is similar to that of Li-S battery. Two typical plateaus at separately 2.35 and 2.10 V for both batteries are observed in discharge process, which can be attributed to a two-step reaction of sulfur with lithium [24]. The similarity of voltage profile demonstrates the electrochemical feasibility of Li-B alloy anode and more remarkably, the electrochemical inertness of Li_7B_6 constituent. Furthermore, the significantly higher discharge potential plateau of LiB-S battery manifests that Li-B alloy is superior to metallic lithium in terms of reducing electrochemical polarization. Besides, the OCVs (at selective SOCs) of LiB-S cell make little difference to those of Li-S cell after standing for some time, better verifying that its increased cell's discharge voltage is mainly because of the polarization reduction during cycling.

The discharge specific capacity and Coulombic efficiency of both cells were plotted versus cycle number in Fig. 3b. The initial discharge specific capacity of LiB-S battery is 1072 mAh g^{-1}$_{sulfur}$, suffering a short period of capacity fading and reaching a plateau of ca. 750 mAh g^{-1}$_{sulfur}$ at 30th cycle. Finally it retains a reversible capacity of 694 mAh g^{-1}$_{sulfur}$ after 100 cycles with a retention rate of 65%, losing only 56 mAh g^{-1}$_{sulfur}$ in the following 70 cycles. The Coulombic efficiency is approximately 100% during the long-term cycle. By contrast, the initial discharge specific capacity of Li-S battery is, higher than LiB-S battery, 1150 mAh g^{-1}$_{sulfur}$. And yet the downward trend doesn't slow until the discharge specific capacity drop to 580 mAh g^{-1}$_{sulfur}$ at 100th cycle, only 50% of the initial value. In addition, the specific capacity and Coulombic efficiency have obvious fluctuations after 40 cycles.
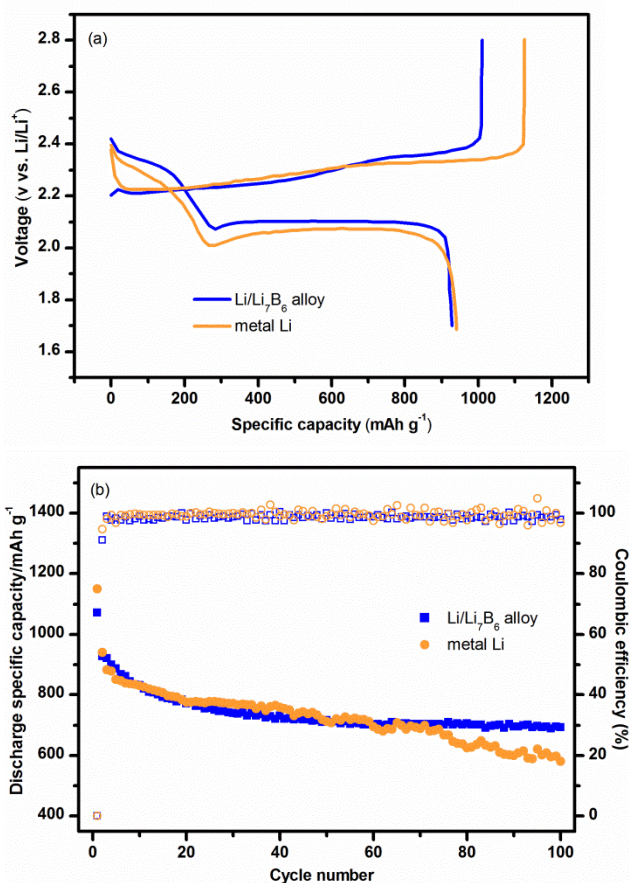
Fig.3 (a) The 1st charge-discharge profiles and (b) cycling performance of Li-B alloy (30wt% B) and metal Li anodes.

SEM images of anodes were obtained after 50 charge/discharge cycles. The metal Li electrode exhibits clear dendritic growth behaviour and cracks formation (Figure 4a), but no dendritic Li and crack can be observed on Li-B alloy (Figure 4b). This result demonstrates that lithium tend to deposition uniformly on the surface of Li-B alloy, which can induce an even current distribution, suppress dendritic Li electrodeposits, and therefore improve safety performance. Also, the avoidance of dendrite formation and pulverization can achieve cycling performance enhancement, because such morphology changes will increase the exposed surface area of anodes, arouse more consumption of electrolyte and finally results in the degradation of the cell performance.
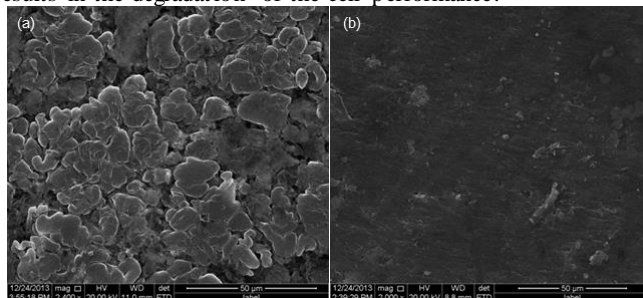
Fig.4 SEM images of (a) metal Li and (b) Li-B alloy (30wt% B) anode after 50 cycles.

Further, we introduced 3 types of alloy with increasing B content, 20wt%, 30wt% and 40wt%, corresponding free Li content of 65wt%,

47wt% and 30wt%, respectively. In has been known that Li-B alloy can induce an even current distribution, suppress dendritic Li electrodeposits and improve cycling performance, here we will discuss the effect of B content on these aspects.

The charge/discharge profiles of various anodes are shown in figure 5. Batteries were cycled with high sulfur loading cathode (4.25mg cm^{-2}) at a current density of 300mA g$^{-1}_{sulfur}$. Alloy containing 40wt% B precedes others, showing the highest specific capacity. Li-B with 30wt% B also performs well, while the Li-B with 20wt% B is poor, even worse than metallic lithium. Alloys with higher content of boron possesses more developed fibrillar network framework, and then enables free Li to have larger specific area. Therefore we can confidently deduce that effective current density was efficiently reduced by the framework structure of Li$_7$B$_6$ compound, and that this function would be more valid with higher content of Li$_7$B$_6$ compound. However, once the content of B is as low as 20wt%, the role of specific surface area enlargement cannot be brought into play because of the high ratio of free Li. Additionally, it has consistently been identified in many studies on Li metal anodes that the morphology of the Li deposit critically depends on the current density, in that dendrite formation is more pronounced at higher current densities[25-27], then this can explain the fact that Li-B alloy has compact and smooth surface after charge/discharge cycles (Figure 4b).
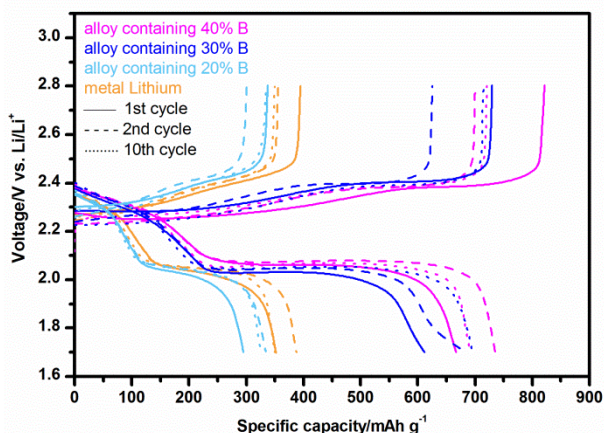
Fig.5 The 1st, 2nd and 10th cycles charge-discharge profiles of 3 types of Li-B alloys and metal Li anodes.

We also used electrochemical impedance spectroscopy (EIS) measurements to study the interface stability of alloy during dissolution/deposition cycling in rich electrolyte system. 0.1M Li$_2$S$_5$ was added into the electrolyte by controlling the stoichiometric ratio of sulfur and lithium sulfide to simulate the electrochemical environment in lithium/sulfur battery. It should be noted that the EIS data in electrolyte without Li2S5 showed larger resistance for all the 4 cells, and the distinction of Li-B alloy was more evident than metal Li. Xiong et al. [28] claimed that polysulfides in the electrolyte solution play an important role for the stability of the interface on the lithium electrode. Here we got a consistent conclusion which is more applicable for Li-B alloy. As shown in Fig.6, all the cells with alloy electrodes have lower resistivity (Figure 6a-c) than that of the one with metal Li electrode (Figure 6d). And the charge-transfer resistances decrease both before and after dissolution/deposition cycle with the increase of boron content. The resistance of SEI layer on Li-B with 40wt% B after 20 cycles is only half of that of metal Li. This is partly because that Li$_7$B$_6$ has a good conductivity (1.43×10^{3}Ω^{-1} cm^{-1}) and a

high Li ion diffusion rate comparative to metallic lithium[29]. Meanwhile the increased specific area of free Li facilitates the speedy formation of SEI layers with better ionic transfer channel.
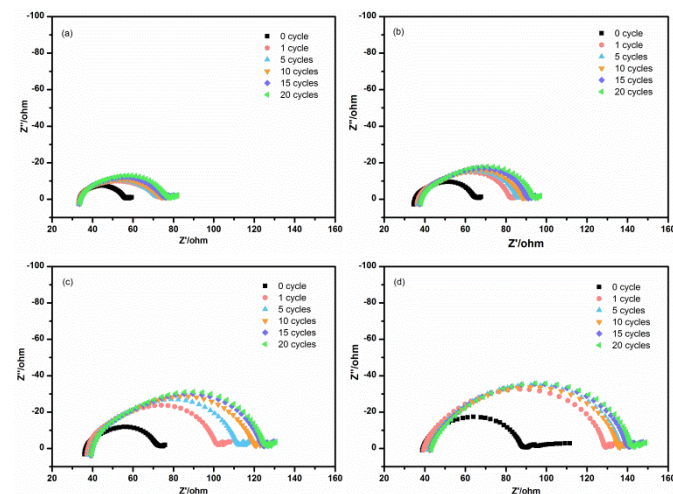
Fig.6 Impedance spectra of (a) Li-B alloy containing 40% B, (b) Li-B alloy containing 30% B, (c) Li-B alloy containing 20% B and (d) metal Li before and after dissolution/deposition cycling in rich electrolyte system.

From comparison of cross sectional microstructure of deplated alloys (Figure 7), we can visually understand how the framework strengthens the alloy. After dissolution of free Li, the structure of lithium was destroyed, and this evolution may lead to thorough pulverization, just like hard earth turn into desert, as shown in Fig.7d. Li-B alloys (Figure 7a-c), by contrast, maintain the entire structure of Li$_7$B$_6$ constituent after removing the free Li. We likened this characteristic to loofah sponge which can preserve the form and structure after dehydration due to its fiber bundle. Fibrillar network framework can be clearly observed on Li-B alloys with 40wt% B and 30wt% B, but this unique structure is not as obvious as the former two in Li-B alloys with 20wt% B. Because of the sturdy supporting function of Li$_7$B$_6$ framework, Li-B alloy would not deform, volume expand or collapse when suffering electrochemical behaviours, thus produce cycle stability and high security for batteries using Li-B alloy anode.
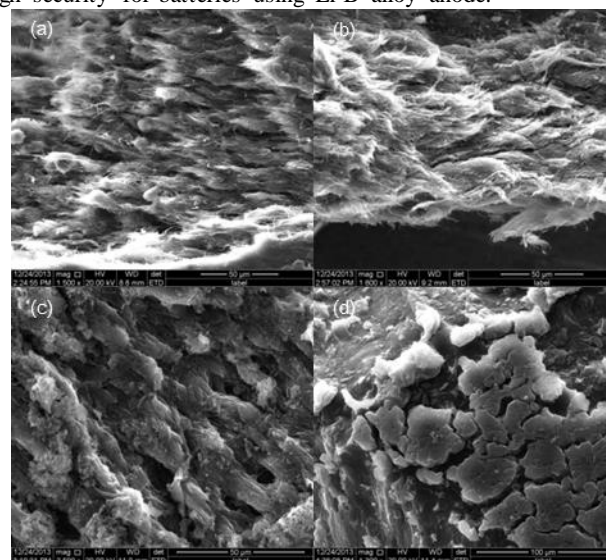
Fig.7 Cross sectional SEM images of (a) Li-B alloy containing 40% B, (b) Li-B alloy containing 30% B, (c) Li-B alloy containing 20% B and (d) metal Li after lithium dissolution.

As mentioned above, Li-B alloy anode possesses preponderance of electrochemical property than metallic Li anode. To have further insight into the mechanism of the superiority of Li-B alloy, X-ray diffraction is used. Figure 8 shows the diffraction scans of Li-B alloys and metal Li before and after Li dissolution/ deposition cycles. The position and strength of all the peaks for Li-B alloy, including Li phase and Li_7B_6 phase, stay largely constant during Li dissolution/ deposition cycles, indicating that such electrochemical behaviour would not impact the multiphase structure of Li-B alloy. However, the result of metallic lithium is essentially different. Two strong peaks at 2θ of 36.2° and 52.0° represent the (110) and (200) peaks of crystalline lithium. The (200) peak of pristine lithium is stronger than (110) peak, yet at the end of Li plating, (110) peak is significantly stronger than (200) peak. The interesting transformation demonstrates orientational crystallization of lithium during the deposition, which could be the underlying reason why metallic Li is prone to form dendrites. On the contrary, crystal form of Li-B alloy kept basically unchanged after electrochemical deposition and dissolution of metallic Li. This marked contrast further verifies that Li-B alloy has advantages in restraining the formation of lithium dendrite. X-ray photoelectron microscopy spectra of cycled alloy anodes were also obtained and peaks attributed to B_2S_3 were found in both element B and S spectra. It demonstrates that boron participates in the formation of SEI film; hence we conjecture that the presence of B_2S_3 may play a positive role during the long-term cycling of Li-S batteries, and the next step in our work will deliver more in-depth insight into this phenomenon.
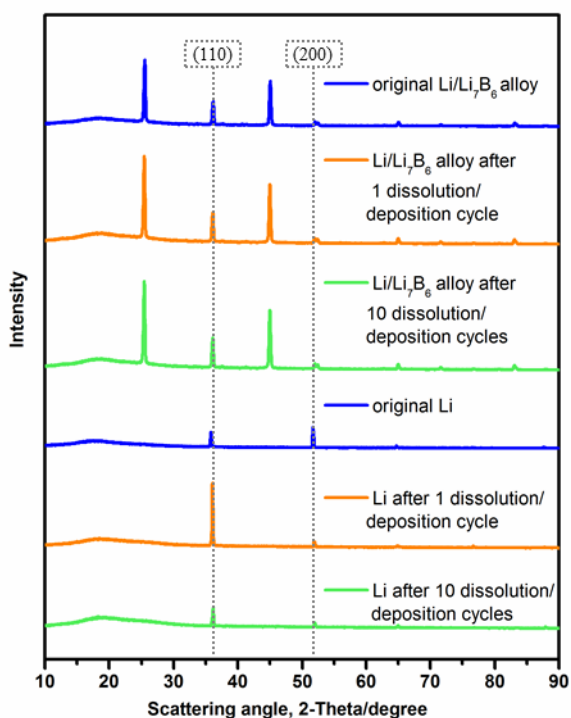
Fig.8 XRD patterns of Li-B alloy (40wt% B) and metal Li electrodes before and after dissolution/deposition cycles.

Conclusions

Li-B alloy was investigated as a potential anode to replace metallic Li for rechargeable lithium batteries. The alloy has unique structure with abundant free Li embedded in stable Li_7B_6 framework. The dissolution/deposition efficiency of Li-B alloy kept highly steady in 100 cycles. The charge/discharge profiles of LiB-S batteries are analogous to Li-S batteries, meaning the electrochemical inertness of Li_7B_6 constituent. Further, the capacity retention for long-term cycles of full cells was greatly improved compared with Li-S batteries. The morphology of Li_7B_6 alloy anode and metallic Li anode demonstrated that Li-B alloy could restrain the formation of lithium dendrite and cracks, which contributed to its high cycle stability and safety performance. It was also proved that more Li_7B_6 constituent could reduce current density on active materials (free Li), and could facilitate the speedy formation of stable SEI layers to a larger degree. Along with the cross sectional microstructure of deplated alloys with varying contents of Li_7B_6, we further confirmed the supporting function of Li_7B_6 loofah sponge-like framework, so that Li-B alloy would not deform, volume expand or collapse when cycling. XRD patterns of Li-B alloy and metallic lithium during dissolution/deposition cycles were firstly presented. The position and strength of all the peaks for Li-B alloy were almost invariable, but those of lithium transformed in a regular manner, demonstrating orientational crystallization.

Acknowledgements

Notes and references

[a] Department of Material Science and Engineering, Beijing University of Chemical Technology, Beijing 100029, China. E-mail: huangyaqin9@gmail.com; Fax: +86-10-64438266; Tel: +86-10-64438266

[b] Military Power Sources Research and Development Centre, Research Institute of Chemical Defense, Beijing 100083, China. E-mail: wangweikun2002@163.com; Fax: +86-10-66748499; Tel: +86-10-66705840

1   Dunn B, Kamath H and Tarascon J M, *Science*, 2011, **334**, 928.

2   Chen H, Cong T N, Yang W, Tan C, Li Y and Ding Y, *Progress in Natural Science*, 2009, **19**, 291.

3   Whittingham M S, *Mrs Bulletin*, 2008, **33**, 411.

4   Medina P, Bizuayehu A W, Catalao J P S, Rodrigues E M G and Contreras J, *2014 47th Hawaii International Conference on. IEEE*, 2014, 2295.

5   Thackeray M M, Wolverton C and Isaacs E D, *Energy & Environmental Science*, 2012, **5**, 7854.

6   Ji X, Nazar L F. *Journal of Materials Chemistry*, 2010, **20**, 9821.

7   Bruce P G, Freunberger S A, Hardwick L J and Tarascon J M, *Nature materials*, 2012, **11**, 19.

8   Song M K, Cairns E J and Zhang Y, *Nanoscale*, 2013, **5**, 2186.

9   Bresser D, Passerini S and Scrosati, *Chem. Commun.*, 2013, **49**, 10545.

10 Zhang S S, *Journal of Power Sources*, 2013, **231**, 153.

11 Miao L X, Wang W K, Wang A B, Yuan K G and Yang Y S, *Journal of Materials Chemistry A*, 2013, **1**, 11659.

12 Wu F, Magasinski A and Yushin G, *Journal of Materials Chemistry A*, 2014, **2**, 6064.

13 Chung S H, Manthiram A, *Chemical Communications*, 2014, **50**, 4184.

14 Fedorková A, Oriňáková R, Čech O and Sedlaříková M, *International Journal of Electrochemical Science*, 2013, **8**, 10308.

15 Yang Y, Zheng G, Cui Y, *Chemical Society Reviews*, 2013, **42**, 3018.

16 D. Aurbach and Y. Cohen, *Journal of The Electrochemical Society*, 1996, **143**, 3525.

17 D. Aurbach, E. Zinigrad, Y. Cohen, and H. Teller, *Solid State Ionics*, 2002, **148**, 405.

18 Kim H, Jeong G, Kim Y U, Kim J H, Park C M and Sohn H J, *Chemical Society Reviews*, 2013, **42**, 9011.

19 Y. M. Lee, N. Choi, J. H. Park, and J. Park, *Journal of Power Sources*, 2003, **964**, 119.

20 Kim H, Lee J T, Lee D C, Oschatz M, Cho W I, Kaskel S and Yushin G, *Electrochemistry Communications*, 2013, **36**, 38.

21 Zhang S S, *Electrochimica Acta*, 2012, **70**, 344.

22 Liang X, Wen Z, Liu Y, Wu M, Jin J, Zhang H and Wu X, *Journal of Power Sources*, 2011, **196**, 9839.

23 Duan B, Wang W, Zhao H, Wang A, Wang M, Yuan K, Yu Z and Yang Y, *ECS Electrochemistry Letters*, 2013, **2**, A47.

24 Yamin H, Gorenshtein A, Penciner J, Sternberg Y and Peled E, *Journal of the Electrochemical Society*, 1988, **135**, 1045.

25 Aurbach D, Zinigrad E, Teller H and Dan P, *Journal of The Electrochemical Society*, 2000, **147**, 1274.

26 Park M S, Yoon W Y, *Journal of power sources*, 2003, **114**, 237.

27 Rosso M, Gobron T, Brissot C, Chazalviel J N and Lascaud S, *Journal of power sources*, 2001, **97**, 804.

28 Xiong S, Xie K, Diao Y and Hong X, *Journal of Power Sources*, 2013, **236**, 181.

29 D. Zhou, Z. Liu, X. Lv, G. Zhou, and J. Yin, *Electrochimica Acta*, 2006, **51**, 5731.

Li-B alloy has **uniform Li depositing morphology** and **offers better capacity retention** as advantageous anode over the metallic lithium.